Biased signalling is an essential feature of TLR4 in glioma cells

Biased Signalling is an Essential Feature of TLR4 in Glioma Cells

Marie-Theres Zeuner[1], Carmen L Krüger[2], Katharina Volk[3], Karen Bieback[4], Graeme S Cottrell[5], Mike Heilemann[2] and Darius Widera[1,*]

[1] Stem Cell Biology and Regenerative Medicine, School of Pharmacy, University of Reading, Reading, United Kingdom

[2] Institute of Physical and Theoretical Chemistry, Johann Wolfgang Goethe-University, Frankfurt, Germany

[3] Department of Cell Biology, University of Bielefeld, Bielefeld, Germany

[4] Institute of Transfusion Medicine and Immunology, Medical Faculty Mannheim, Heidelberg University, Heidelberg, Germany

[5] Cellular and Molecular Neuroscience, School of Pharmacy, University of Reading, Reading, United Kingdom

* To whom correspondence should be addressed:
Dr Darius Widera
Reading School of Pharmacy, University of Reading, PO Box 226, Whiteknights, Reading, RG6 6AP, United Kingdom
E-mail: d.widera@reading.ac.uk

Abstract

A distinct feature of the Toll-like receptor 4 (TLR4) is its ability to trigger both MyD88-dependent and MyD88-independent signalling, culminating in activation of pro-inflammatory NF-κB and/or the antiviral IRF3. Although TLR4 agonists (lipopolysaccharides; LPSs) derived from different bacterial species have different endotoxic activity, the impact of LPS chemotype on the downstream signalling is not fully understood. Notably, different TLR4 agonists exhibit anti-tumoural activity in animal models of glioma, but the underlying molecular mechanisms are largely unknown.

Thus, we investigated the impact of LPS chemotype on the signalling events in the human glioma cell line U251. We found that LPS of *Escherichia coli* origin (LPS_{EC}) leads to NF-κB-biased downstream signalling compared to *Salmonella minnesota*-derived LPS (LPS_{SM}). Exposure of U251 cells to LPS_{EC} resulted in faster nuclear translocation of the NF-κB subunit p65, higher NF-κB-activity and expression of its targets genes, and higher amount of secreted IL-6 compared to $LPS_{SM.}$ Using super-resolution microscopy we showed that the biased agonism of TLR4 in glioma cells is neither a result of differential regulation of receptor density nor of formation of higher order oligomers. Consistent with previous reports, LPS_{EC}-mediated NF-κB activation led to significantly increased U251 proliferation, whereas LPS_{SM}-induced IRF3 activity negatively influenced their invasiveness. Finally, treatment with methyl-β-cyclodextrin (MCD) selectively increased LPS_{SM}-induced nuclear translocation of p65 and NF-κB activity without affecting IRF3.

Our data may explain how TLR4 agonists differently affect glioma cell proliferation and migration.

Keywords

TLR4, LPS, NF-kappaB, IRF3, inflammatory balance, biased agonism

1. Introduction

Toll-like receptors (TLRs) are a group of pattern recognition receptors (PRRs) responsible for detection of pathogen-associated molecular patterns (PAMPs) and damage-associated molecular patterns (DAMPs) (reviewed in [1]). TLR4 is the most extensively studied TLR and recognises lipopolysaccharides (LPSs) that are outer surface compounds of gram-negative bacteria [2, 3]. Prior to receptor binding, LPS forms a complex with LPS-binding protein. Activation of TLR4 is further facilitated by accessory co-receptors cluster of differentiation 14 (CD14), and myeloid differentiation protein-2. Ligand binding induces TLR4 dimerisation which in turn leads to recruitment of adaptor proteins Myeloid differentiation primary response gene 88 (MyD88) or Toll-interleukin receptor-domain-containing adapter-inducing interferon-β

(TRIF), that determine the downstream signalling pathway [4, 5]. In particular, recruitment of MyD88 leads to activation of the pro-inflammatory transcription factor nuclear factor kappa-light-chain-enhancer of activated B cells (NF-κB). This is preceded by phosphorylation and proteasomal degradation of the inhibitory IκB proteins. On the other hand, assembly of TRIF and TRIF-related adaptor molecule [5, 6] is independent of MyD88 and activates the transcription factor interferon regulatory factor 3 (IRF3) [7, 8]. The subsequent DNA-binding of IRF3 induces expression of type I interferons (IFNα, IFNβ) [9]. The IRF3 target gene IFNβ exhibits not only anti-viral but also anti-inflammatory properties [10]. Notably, compensatory induction of anti-inflammatory factors following the initial pro-inflammatory phase plays a central role in resolving acute inflammation caused by LPS [11, 12].
In addition to immune cells, functional TLR4 is constitutively expressed within most cell types of the central nervous system including neural stem cells, microglia, neurons, astrocytes, and neural stem cells [13-17]. In particular, TLR4 is involved in development of the nervous system [18, 19] and regulates differentiation and proliferation of adult neuronal precursor cells [14]. It has been reported that both the intracranial challenge with LPS_{EC} and the intraperitoneal infection with *E. coli* lead to secretion of pro-inflammatory cytokines such as interleukin 6 (IL6) in mouse brain [15]. Similar to astrocytes, primary glioblastoma cells and glioblastoma cell lines express functional TLR4 [20-22]. Interestingly, studies on LPS-mediated activation of TLR4 in glioblastoma cells *in vitro* and *in vivo* revealed largely conflicting outcomes ranging from significant anti-tumoural action to tumour-promoting effects [21, 23].

To date, the exact mechanisms used by TLR4 to regulate ligand-dependent downstream signalling events remain unidentified. In 2004, Saitoh and colleagues suggested that oligomerisation may play a role in ligand biased TLR4-mediated signalling [24]. Furthermore, cholesterol-rich plasma membrane microdomains are known to regulate TLR4 oligomerisation [25]. However, the impact of microdomains on TLR4 signalling in non-hematopoietic cells including cancer cells is unclear.

Since different LPS chemotypes exert different endotoxic activity and seem to have diverse impact on glioblastoma, we aimed to elucidate the underlying molecular mechanisms and challenged the human glioma cells line U251 with LPS_{EC} and LPS_{SM}. We present evidence that TLR4 activation by LPS derived from LPS_{EC} or LPS_{SM} differently affects the inflammatory balance between NF-κB and IRF3. We also demonstrate that the dynamics and kinetics of NF-κB and IRF3 activation is ligand-specific. We further show that the differences in downstream signalling are not dependent on receptor oligomerisation or receptor density. Finally, our data suggests that the discrimination between LPS chemotypes is membrane microdomain dependent.

2. Materials and Methods

2.1. Cell culture and LPS treatment

Human glioblastoma cell line U251 (Cell Line Service, Eppelheim, Germany) was cultivated in antibiotic/antimycotic-free Dulbecco's Modified Eagle's Medium (DMEM) high glucose (Sigma-Aldrich, cat. No. D5671, Taufkirchen, Germany) supplemented with 1% L-glutamine (200 mM; Sigma-Aldrich) and 10% heat-inactivated fetal calf serum (FCS, lot: 126K3398, Sigma-Aldrich) (hereinafter referred to normal culture medium) in a humidified incubator (Binder, Tuttlingen, Germany) at 37°C and 5% CO_2. Ultrapure LPS from *Salmonella minnesota* (Ultrapure *S. minnesota* R595, InvivoGen, Toulouse, France) and *E. coli* (Ultrapure *Escherichia coli* K12, InvivoGen) were dissolved in endotoxin-free water. U251 cells were grown in normal culture medium prior to 4 h starvation by replacing the medium with normal medium without FCS. For super-resolution microscopy, starvation was performed 12 h prior to treatment. Afterwards, U251 cells were treated with respective LPS chemotype.

2.2. Transient transfection and gene reporter assays

Transfection of glioblastoma cell lines was performed using Amaxa™ RatNSC Nucleofector™ Kit (Lonza Group AG, Basel, Switzerland) and the Amaxa™ Nucleofector II device (Lonza Group, Basel, Switzerland) according to manufacturer's guidelines. Briefly, 5 $\times 10^6$ cells were mixed with Nucleofector solution containing pmaxGFP (Lonza) and pRL-CMV (Promega, Mannheim, Germany). For NF-κB reporter gene assays, TK $(NF\text{-}\kappa B)_6$LUC [26] vector and for IRF3 reporter gene assays IRF-3-Gal4 (pEFGal4−IRF-3) and UAS-LUC vectors (p-55UAS_GLuc, kindly provided by K. Fitzgerald, University of Massachusetts Medical School, Worcester, USA) were used. Expression of pmaxGFP was confirmed via confocal scanning microscopy (LSM 510, Carl Zeiss, Jena, Germany) 24 h after transfection. Cells were exposed hereinafter to LPS for 48 h. Transcription factor (NF-κB or IRF3)-dependent *firefly*-luciferase activity versus transcription factor independent *Renilla* luciferase measurement was performed using Dual-Luciferase® Reporter Assay System (Promega Corporation, cat. no. E1960) according to manufacturer's guidelines on a Lumat device (Berthold Technologies, Bad Wildbach, Germany).

2.3. Immunocytochemistry and visualisation of membrane microdomains

U251 cells were cultivated in 12-well plates on microscope coverslips, serum starved, stimulated with LPS (see above, (0-24 h)) and fixed in PBS containing 4% paraformaldehyde (4% PFA, 20 min, 4°C). For TLR4 staining 4% PFA solution was supplemented with 320 mM sucrose. Cells were then permeabilised and blocked in PBS containing 0.02% Triton-X-100 (Sigma-Aldrich, cat. No. T8787) and 5% normal goat serum (Dianova, Hamburg, Germany).

Cells were stained for p65 (1:100, sc-8008, Santa Cruz Biotechnology, Heidelberg, Germany), IRF3 (1:50, sc-9082, Santa Cruz Biotechnology) or TLR4 (1:100, sc-10741, Santa Cruz Biotechnology) followed by incubation with respective secondary fluorochrome-conjugated antibodies (AlexaFluor555 or AlexaFluor488, Thermo Fisher Scientific, Waltham, MA, USA, 1:300). Nuclei were stained using DAPI (1:2000, Life Technologies, Darmstadt, Germany). For membrane microdomain visualisation, cells were incubated with AlexaFluor488 conjugated Cholera Toxin subunit B (CTx, 1:100, 10 min, room temperature, Thermo Fisher Scientific). Imaging was performed using confocal laser scanning microscopy (CLSM (LSM 780, Carl Zeiss, Jena, Germany)). Fiji was used for image processing, co-localisation (colocalization threshold) analysis and pixel intensity measurements [27].

2.4. Membrane microdomain disruption

For membrane microdomain disruption, cells were treated with 10 mM MCD (30 min, Sigma-Aldrich) and washed with normal medium twice prior to further experimentation.

2.5. Flow cytometry

For flow cytometric analysis of TLR4 expression, cells were harvested using Accutase and fixed as a single cell suspension in 4% PFA supplemented containing 320 mM sucrose (15 min, room temperature), followed by blocking with 10% FcR blocking reagent (Miltenyi Biotec, Bergisch Gladbach, Germany) and incubation with anti-TLR4 antibody (Santa Cruz Biotechnology, 1:100, 1 h, room temperature). Phycoerythrin (PE)-conjugated goat-anti rabbit IgG was used for detection. Detection was performed on a CyFlow Space flow cytometer (Partec, Muenster, Germany).

2.6. Western blotting

To establish a low baseline of active NF-κB, cells were serum-starved for 4 h and subsequently incubated in fresh FCS-containing medium with or without LPS for the indicated time points. Unstimulated cells (for each time point) served as control for quantification. Stimulated and unstimulated U251 cells were washed with PBS after the indicated time points and lysed in RIPA buffer containing proteinase inhibitors (Roche, UK). Cell lysates were incubated (4°C, 1 h), centrifuged (13000 *g*, 15 min) and boiled (95°C, 10 min) following addition of reducing sample buffer. Samples were separated by SDS-PAGE and transferred to PVDF membrane (10600029, GE Healthcare, Chalfont St. Giles, UK). Membranes were incubated in PBS for 10 min, blocked in 5% BSA in PBS supplemented with Tween 20 (PBST) for 1 h and incubated with primary antibodies: 14-3-3-ζ (1:4000, sc-1019, Santa Cruz Biotechnology) or IκBα (1:1000, ab32518, Abcam, UK) in 5% BSA in PBST for 1.5 h. After washing with PBST, membranes were incubated in secondary antibody (goat anti-rabbit IgG HRP (Sigma-Aldrich, GERPN2108, 1:5000)) for 1 h. Immunoreactive proteins were detected using

chemiluminescence (ECL Reagent, Sigma-Aldrich, GERPN2108) and visualized using an ImageQuant LAS 4000 mini device (GE Healthcare). Fiji was used for image processing and densitometric analysis. Relative IκB protein amount was calculated as a ratio of IκB/14-3-3-ζ and normalised to the untreated control for each time point.

2.7. RNA isolation and cDNA synthesis

Total RNA from U251 cells was isolated using a NucleoSpin 8 core kit (Macherey-Nagel, Düren, Germany) according to manufacturer's guidelines. cDNA synthesis was performed using First Strand cDNA Synthesis Kit (Thermo Fisher Scientific, cat. No. K1612, Darmstadt, Germany) according to manufacturer's guidelines.

2.8. RT-qPCR

qPCR was performed using PerfeCTa® SYBR® Green SuperMix (Quanta BioSciences, Gaithersburg, USA) and measured in a Rotor Gene 6000 (QIAGEN, Hilden, Germany) according to respective manufacturer's guidelines. The primer sequences (5'-3') were as follows: Tumor necrosis factor α (TNFα) (fwd: CAGAGGGCCTGTACCTCATC, rev: GGAAGACCCCTCCCAGATAG), Interleukin 8 (IL8), (fwd: GTGCAGTTTTGCCAAGGAGT, rev: CTCTGCACCCAGTTTTCCTT), IFNβ (fwd: TGCTCTCCTGTTGTGCTTCT, rev: AGCTGCTTAATCTCCTCAGGG), GAPDH (fwd: CATGAGAAGTATGACAACAGCCT, rev: AGTCCTTCCACGATACCAAAGT), PPIA (fwd: CAAGCATGTGGTGTTTGGCA, rev: TGGTCTTGCCATTCCTGGAC), PGK1 (fwd: GACAATGGAGCCAAGTCGGT, rev: TCTGGGCCTACACAGTCCTT), and PPIB (fwd: AGATGTAGGCCGGGTGATCT, rev: CTCCGCCCTGGATCATGAAG). Relative expression was calculated using the equation of mathematical delta-delta method. Since activation of TLR4 can result in a regulation of several widely used reference genes [28], additional control qPCRs using GAPDH, PPIA, PGK1, and PPIB were performed (Fig S4).

2.9. ELISA

U251 cells were grown in 96-well plates in normal culture medium, starved and treated with LPS. Supernatants were collected, centrifuged (5000 *g*, 5 min, 4°C) and IL-6 quantified using the Human IL-6 DuoSet ELISA (RnD Systems, cat. No. Dy206, Abingdon, United Kingdom) according to manufacturer's guidelines.

2.10. Proliferation assay

U251 cells were grown in a 12-well plate in normal culture medium with and without LPS. Cells were detached using trypsin/EDTA after 3 days of incubation in a humidified incubator at 37 °C and 5 % CO_2. Cells numbers were assessed using a Neubauer improved cell counting chamber (Carl Roth, Karlsruhe, Germany) and the EVOS XL digital inverse microscope (EVOS

® Cell Imaging Systems, Life Technologies, Darmstadt, Germany). All proliferation assays were performed as a triplicate for each condition followed by statistical evaluation.

2.11. Wound healing assay

The *in vitro* wound healing assay was performed as described previously in a 24-well plates [29]. Briefly, confluent U251 cells were grown in normal culture medium, starved (4 h) and a vertical scratch made in each well using a small plastic pipette tip followed by a careful washing step with starving medium. The medium was replaced with normal culture medium containing either LPS_{SM} or LPS_{EC}. The region of the scratch was defined by reference markings and documented using an inverse microscope 30 min and 8 h after the scratch. Image analysis was performed using Fiji.

2.12. Immunolabelling for super-resolution imaging

Cells were washed with pre-warmed 400 mM sucrose solution (Merck, Germany) prior to incubation in fixation buffer containing 4% formaldehyde (methanol-free, Thermo Fisher Scientific), 0.2% glutaraldehyde (Sigma-Aldrich, USA) and 400 mM Sucrose for 15 min. After extensive washing in PBS, blocking was performed using 2% BSA (Sigma, Germany) for 30 min. Mouse monoclonal antibody against human TLR4 (Santa Cruz Biotechnology, USA) in 2% BSA over night at room temperature (2 µg/ml) was used for immuno-labelling of the samples. For control measurements, mouse monoclonal anti-human TLR4 (ab22048, Abcam, UK) was applied for 1 h at room temperature (0.1 µg/ml). After 3 washing steps with PBS, AlexaFluor647 coupled F(ab')2 goat anti-mouse IgG antibody (A-21237, Life Technologies, USA) was used as secondary antibody (4 µg/ml; diluted in 2% BSA solution) and incubated for 1 h, followed by three washing steps in PBS.

2.13. Super-resolution imaging

A custom-built setup was used, as previously described by Fricke *et al.* [30]. Briefly, excitation laser lines (405 nm (CUBE 405-50C, Coherent, USA), 643 nm (diode laser, iBEAM smart, Toptica, Germany)) were aligned with appropriate dichroic mirrors, passed an acousto-optic tuneable filter (AAOptics, France) and were focused on the back focal plane of an Olympus IX-71 inverted microscope equipped with a 100 × oil immersion objective (PLAPO 100× TIRFM, NA ≥ 1.45, Olympus). A nose piece (Olympus, Japan) was implemented to minimize mechanical drift. Fluorescence was detected on an EMCCD camera (iXon3, Andor, UK). Imaging was performed in 100 mM β-mercaptoethylamine (MEA (Sigma; Germany)) in PBS, pH 7.5. 20 000 frames were recorded using an integration time of 30 ms under continuous 643 nm laser illumination at intensity densities of 2 – 2.5 kW/cm². Photoswitching of Alexa Fluor647 was induced by low-intensity irradiation with 405 nm at well-defined time points in order to achieve an optimal density of active single molecules during the experiment.

2.14. Data analysis of super-resolved images

Super-resolved images were reconstructed using rapi*d*STORM [31]. Cluster analysis was performed using Ripley's H -function in a custom-written software [32]. Analysis was performed for 13 cells for each condition; five regions of interest (ROIs) with a size of 2 × 2 μm² were selected for each cell.

Morphological cluster analysis was performed using the image-based cluster analysis plugin 'Analyze Particles' implemented in Fiji. The number of TLR4 clusters and their area on the cell membrane was extracted, as well as the particle number per μm² (Fig. S2, Table 1 and S1).

2.15. Statistical analysis

GraphPad Prism software (GraphPad Software, La Jolla, CA, USA) was used to perform statistical analysis. For statistical comparison, unpaired students t-test (two tailed, confidence interval 95%) or one-way analysis of variance with Bonferroni's correction (confidence interval 95%) was performed (when appropriate). A value of $p<0.05$ was considered as significant. All results were obtained from at least three independent experiments.

3. Results

3.1. Clusters of TLR4 are uniformly distributed in the membrane of U251 cells

Flow cytometry was used to confirm expression of TLR4 in U251 cells. In agreement with previous studies demonstrating expression of TLR4 in various glial cells [33], we detected high levels of cell-surface TLR4 in the U251 cell line (Fig. 1A). We applied single-molecule localization microscopy (SMLM, [34]) to determine the nano-spatial organization of TLR4 at the cell-surface of unstimulated cells. Specifically, we used direct stochastic optical reconstruction microscopy (*d*STORM) [35] to visualize immuno-labelled TLR4 (Fig. 1B). Individual TLR4 clusters on the cell membrane were resolved and a localization precision of 8.9 - 10.3 nm was determined (Fig. S1) using nearest neighbour analysis [36]. We found that TLR4 is uniformly distributed across the whole plasma membrane and exhibits a density of 7.0 ± 1.0 receptor clusters / μm^2 (Fig. 1B).

3.2. Kinetics of TLR4-induced nuclear translocation of IRF3 and NF-κB are ligand-dependent

The downstream signalling cascades activated by LPS chemotypes was investigated using immunocytochemical assessment of nuclear NF-κB subunit p65 (Fig. 2). Treatment with LPS_{EC} promoted rapid nuclear translocation of p65 (30 min, peak at 2h) compared to LPS_{SM} where only low levels of nuclear NF-κB were observed at 2 h. Through the time course, the nuclear

translocation of p65 in cells treated with LPS_{SM} was significantly lower compared to LPS_{EC}-treated cells. In contrast, the levels of nuclear IRF3 were significantly higher in LPS_{SM}-treated cells in comparison to LPS_{EC} at both 4 and 24 h.

3.3. LPS_{EC} leads to a fast degradation of IκBα

Degradation of its cytoplasmic inhibitor IκBα is mandatory for nuclear translocation of NF-κB [37]. In order to investigate potentially different degradation kinetics of IκB-protein after treatment, total levels of the IκBα protein were analysed using Western blot. To determine the level of basal IκB degradation after re-exposure of the cells to serum, relative IκBα-protein amount was assessed in unstimulated cells at all time points (Fig. 3A). Relative IκB after exposure to LPS_{SM} or LPS_{EC} was normalised to unstimulated cells at the respective time points (Fig. 3B). A significant reduction of IκBα-protein amount was observed in lysates of cells stimulated with LPS_{EC} for 2 h, whereas no differences were detected between control and LPS_{SM}-treated cells (Fig. 3B).

3.4. Levels of TLR4-induced IRF3 and NF-κB activity are ligand dependent

To measure the sustained induction of NF-κB, and IRF3 activity, we transiently transfected U251 with NF-κB and IRF3 reporter plasmids. Here, we observed a significantly higher NF-κB activity in LPS_{EC} treated cells (Fig. 3C, LPS_{EC}: 12.2 ± 2.0 fold, LPS_{SM}: 7.96 ± 2.1 fold increase of relative NF-κB activity compared to control). In contrast, no significant difference was detected in the relative IRF3 activity (Fig. 3C).

3.5. Different LPS chemotypes differentially affect the expression level of NF-κB and IRF3 target genes

Activation of NF-κB and IRF3 results in transcription of the respective target genes. Thus, RT-qPCR was applied to investigate a potential regulation of the IRF3 target gene IFNβ, and TNFα, IL8 as targets of NF-κB. Cells were treated with LPS_{SM} or LPS_{EC} for 1 h or 24 h, respectively. In order to exclude potential regulation of the reference gene GAPDH, control qPCRs were performed using PGK1, PPIA, and PPIB as a reference. In U251, no LPS-dependent regulation was observed for all reference genes in all experimental conditions (Fig. S4). In contrast, we observed a significantly stronger induction of NF-κB targets TNFα (3.54 ± 1.46 fold) and IL8 (3.07 ± 0.27 fold) after treatment with LPS_{EC} (Fig. 3D) compared to control. In contrast, upregulation of the IRF3 target gene IFNβ was observed only in cells treated with LPS_{SM} for 24 h (2.02 ± 0.34 fold, Fig. 3E).

3.6. Levels of IL6-secretion after TLR4-activation depend on LPS chemotype

ELISA was applied to quantitatively measure LPS-induced secretion of the pro-inflammatory IL6 (Fig. 3F). Here, we were able to detect low levels of IL6 after 4 h of stimulation with both

LPS chemotypes ($LPS_{EC:}$ 804.73 ± 114.33 pg/ml; LPS_{SM}: 449.03 ± 272.83 pg/m). Notably, significantly higher levels of IL6 were secreted after stimulation with LPS_{EC} (5810.27 ± 1062.36 pg/ml) for 24 h compared to LPS_{SM} (2571.12 ± 156.18 pg/ml).

3.7. LPS_{EC} but not LPS_{SM} promotes proliferation of U251 cells

Proliferation of glioma cells is known to be largely NF-κB dependent [38]. In order to investigate if the differential NF-κB activity in LPS_{EC} and LPS_{SM}-treated cells correlates with their proliferative behaviour, total cell number was determined (Fig. 3G). Here, significantly higher cell numbers were measured after treatment with LPS_{EC} for 72 h ($1.1 \times 10^5 \pm 3.45 \times 10^4$) compared to both LPS_{SM}-treated ($6.67 \times 10^4 \pm 2.71 \times 10^4$) and control cells ($6.67 \times 10^4 \pm 1.57 \times 10^4$).

3.8. Migration of glioma cells is inhibited by LPS_{SM} but not by LPS_{EC}

It has previously been shown that migration of glioblastoma cells is NF-κB-dependent [39] and that an active IRF3 inhibits their migration [40]. To test the impact of differential NF-κB and IRF3 activity on U251 migration, wound healing assays were performed. Cells were exposed to LPS_{EC} or LPS_{SM} and allowed to migrate for 8 h. Quantification of the coverage area (Fig. 3H) revealed no significant differences in migratory behaviour of cells treated with LPS_{EC} (51.81 ± 1.46 %) in comparison to the control (70.22 ± 18.79 %). In contrast, a strong inhibitory effect was observed if LPS_{SM} was applied (26.92 ± 6.46 % coverage, Fig. 3H).

3.9. LPS chemotype affects TLR4 cluster distribution

It has been suggested that internalisation and oligomerisation of TLR4 on the cell membrane can influence the shift from pro- to anti-inflammatory signalling [24, 41].

Thus, we used *d*STORM to quantitatively determine the influence of different LPS chemotypes on the spatial distribution, density and clustering behaviour of TLR4 (Fig. 4A). On average 7.0 ± 1.0 (SEM) TLR4 clusters per µm² were found in untreated cells (n=13). For cells treated with either of the two LPS chemotypes and at different incubation time, the average number of receptor clusters did not change significantly (Table 1). A broad distribution of receptor cluster density per µm² was found for most experimental conditions. However, we also observed that 1 h stimulation with LPS_{SM} and 2 h with LPS_{EC} leads to a narrowing of the distribution patterns at lower levels (Table 1, Fig. 4B). In contrast, treatment with LPS_{EC} for 1 h induces in a subpopulation with 10 receptor clusters per µm² (Fig. 4B).

3.10. LPS does not induce higher order TLR4 cluster formation independent on its chemotype

To further investigate the size of TLR4 clusters on the plasma membrane before and after stimulation with different LPS species, we determined the radius of each receptor cluster from

the area of each counted cluster. For each condition, the cluster radii were averaged and determined to range from 26 to 28 nm (Table 2, Fig. 4C). We verified the above results by using a different primary antibody; super-resolution imaging and counting of receptor clusters led to similar results (Fig. S3). As negative control, no primary antibody was applied to the cells and analysis of those measurements resulted in 0.3 ± 0.1 particles per µm² (Fig. S2). Next, Ripley's H-function [32, 42] was applied, which allows a coordinate-based distribution analysis of point distributions, and deliver information on average cluster size. Applied to SMLM data, a uniform distribution of single-molecule localizations results in a horizontal line at zero. Clustering of single-molecule localizations results in an H-function that deviates to positive values, with the maximum reporting on the average cluster size. For each cell and experimental condition, 5 regions of interest were analysed and the H-functions determined for each cell were summed up. Each condition showed a clear maximum between 52 and 58 nm (Tab. 2, Fig. 4D+E). This is consistent with the results on cluster radii obtained from the morphological cluster analysis: if the inter-cluster distance is large compared to the cluster size, the maximum of the H-function reports the cluster diameter [32]. As the overall density of TLR4 receptor clusters is small, the inter-cluster distance is large compared to the cluster sizes. The maximum of the H-function can thus be interpreted as cluster diameter, and values of 52 to 58 nm correspond well to a cluster radius of 26 to 28 nm determined with the morphological cluster analysis. Again, we did not observe a significant change in the size of TLR4 clusters, suggesting that TLR4 is not building higher-order structures in glioma cells after LPS induction.

3.11. MCD treatment significantly increases LPS_{SM} induced NF-κB activity, but neither influences LPS_{EC}-mediated NF-κB activation nor IRF3 activity driven by both LPS chemotypes

As TLR4 oligomerisation is known to be partly dependent on cholesterol-rich membrane microdomains in hematopoietic cells [25], we determined if the same was true in the U251 glioblastoma line. Cells were co-labelled with CTx and an anti-TLR4 antibody (Fig. 5A) followed by CLSM. Here, we detected a partial co-localisation of CTx and TLR4 signal.

In order to investigate the impact of intact microdomains on TLR4-mediated signalling, cells were treated with MCD followed by a wash-out and exposure to both LPS chemotypes. In an alternative approach, cells transiently transfected with NF-κB or IRF3 reporter plasmids were treated with MCD and LPS followed by cultivation, lysis and determination of promotor-driven luciferase bioluminescence. Here, we found a significant increase of TLR4-mediated nuclear translocation of NF-κB after treatment with LPS_{EC} (Fig. 5B). Notably, the amount of nuclear NF-κB in LPS_{SM} / MCD treated cells was significantly higher than both, control / MCD and LPS_{EC} / MCD treated cells. We detected no nuclear translocation induced by MCD-treatment alone. Finally, reporter gene assays revealed a significantly increased NF-κB driven bioluminescence in cells treated with LPS_{SM} and MCD. In particular, microdomain disruption led to an increase

in LPS_{SM}-induced NF-κB activity to a level comparable to the LPS_{EC} approach (Fig. 5C). In contrast, exposure of the cells to MCD had no effect on LPS-induced IRF3 activity (Fig. 5D).

4. Discussion

Unlike all other TLRs, TLR4 is the only TLR family member with the ability to trigger both MyD88-independent and MyD88-dependent pathways after ligand binding [5]. MyD88-dependent signalling culminates in activation of NF-κB, a transcription factor with pro-inflammatory and proliferation inducing properties [43, 44]. In contrast, MyD88-independent pathways mainly activates IRF3 regulating anti-viral and anti-inflammatory signals, including type I interferons [10, 45]. Our results show that U251 cells, a human glioblastoma cell line, express cell-surface TLR4 and for the first time, that stimulation with diverse TLR4-activating LPS species promotes biased activation of NF-κB and IRF3 pathways. In particular, we show using Western blotting and microscopy that LPS_{EC} and LPS_{SM} promote differential activation and nuclear translocation of NF-κB and IRF3. In addition, we observed that differential activation of signalling pathways has consequences on gene transcription and cellular proliferation and migration. Finally, we show that MCD-induced disruption of membrane microdomains is sufficient to induce an increase in LPS_{SM}-induced NF-κB activity to a level comparable to the LPS_{EC} approach.

4.1. U251 cells express TLR4 at the plasma membrane

TLR4 is constitutively expressed in most cells of the central nervous system under physiological conditions, but also in glioblastoma cells [20-22]. As a first step to investigating potential ligand-dependent differences in TLR4-mediated downstream signalling in U251 cells, we first verified TLR4 expression using flow cytometry and *d*STORM imaging. In agreement with the literature [46], we verified that U251 cells express TLR4 at the cell-surface and that the receptor clusters are uniformly distributed (Fig. 1B). In addition to TLR4, U251 cells also express myeloid differentiation protein-2 as well as the intracellular adapter proteins, MyD88 and TRIF, but lack CD14. As CD14 is believed to contribute to the activation of MyD88-independent signalling [47], we performed our experiments in the presence of serum, to provide a source of soluble CD14 [48].

4.2. Diverse LPS species exhibit ligand-specific activation of NF-κB and IRF3 in U251 cells

The kinetics and dynamics of signalling pathways activation can have profound effects on biological function. Indeed, it has been known for some time that biological and synthetic agonists of receptors can act as biased agonists, preferentially activating one signalling pathway over another. The existence of biased agonists is not restricted to one receptor type, with biased agonists now known to exist for G protein-coupled receptors (reviewed in [49, 50],

enzyme-coupled receptors (reviewed in [51, 52] and nuclear receptors [53]. Furthermore, this phenomenon is not restricted to the binding of molecules to the orthosteric site, as allosteric modulators are also known to have diverse effects (reviewed in [54, 55]).

To assess the respective kinetics of NF-κB and IRF3 activation driven by LPS_{EC} and LPS_{SM}, we analysed nuclear translocation of the NF-κB subunit p65 and IRF3. We observed that treatment of U251 with LPS_{EC} promoted faster and stronger nuclear translocation of p65 compared to cells exposed to LPS_{SM}. This result is consistent with the kinetics of IκB degradation following exposure to LPS_{EC} as demonstrated using Western blotting. In parallel, we measured nuclear translocation of IRF3. Stimulation of the cells with LPS_{SM} resulted in an early nuclear translocation of IRF3 and a significantly higher amount of nuclear IRF3 after 24 h. These results suggest that LPS_{EC} and LPS_{SM} shift the inflammatory balance by differentially activating the NF-κB and IRF3 pathways. In support of this observation, vaccine adjuvant monophosphoryl lipid A and synthetic TLR4 agonists have been reported as TRIF-biased agonists of TLR4 [56-58]. In addition, it has been suggested that interferon signalling contributes to the TRIF bias that synthetic lipid A promotes following activation of TLR4 in mouse bone marrow-derived dendritic cells [59]. Interestingly, in hepatocytes IRF3 can directly regulate NF-κB-signalling via a direct binding and inactivation of the upstream kinase IKKβ [60].

Endotoxins from diverse sources including *Neisseria meningitidis*, *E. coli* 55:B5 and *Vibrio cholerae* differentially activate MyD88-dependent and -independent signalling pathways in human and mouse macrophage cells [61]. *N. meningitidi* lipooligosaccharide potently activated both MyD88-dependent and -independent signalling pathways, whereas *E. coli* 55:B5 and *V. cholerae* LPSs selectively induced the MyD88-dependent pathway. Similar to our study, LPS_{SM} was demonstrated to selectively activate the MyD88-independent pathway [61]. Interestingly, very recently, Salyer and colleagues suggested that nystatin and amphotericin B could act as TRIF-biased TLR4 agonists [62].

4.3. Gene expression and secretion is regulated by ligand-specific activation of TLR4

Recently, using a bioinformatical approach, Iwanaszko and colleagues suggested that cross-talk between IRF3 and NF-κB signalling pathways could also occur at the level of target gene promoters [63]. We used luciferase-based gene reporter assays to measure the sustained induction of NF-κB and IRF3. We detected significantly higher levels of NF-κB-driven luciferase in cells exposed to LPS_{EC} in comparison to cells treated with LPS_{SM} and untreated cells. In contrast, no significant differences were observed in cells treated with LPS_{EC} and LPS_{SM} regarding IRF3-driven luciferase activity suggesting a shift towards pro-inflammatory NF-κB signalling in LPS_{EC} treated cells. This shift was further verified by faster degradation of IκBα and higher expression and secretion of pro-inflammatory NF-κB target genes in LPS_{EC} treated

cells. In contrast, LPS_{SM} induced higher expression of IFNβ mRNA. A similar shift in gene transcription was observed in macrophages, with *E. coli* 55:B5 and *V. cholerae* LPSs inducing similar levels of pro-inflammatory TNFα, IL-1β and macrophage inflammatory protein 3α, but significantly less than LPS_{SM}. Conversely, LPS_{SM} induced significantly more IFNβ, nitric oxide and IFNγ-inducible protein 10 than *E. coli* 55:B5 and *V. cholerae* LPSs, confirming the bias of LPS_{SM} towards MyD88-indendepent signalling [61]. Indeed, earlier studies measuring cytokine release using whole blood assays also noted disparate secretion depending on the nature of the purified LPS used for the challenge [64].

A shift in balance between NF-κB and IRF3 towards the anti-inflammatory IRF3 signalling is known to be a feature in regulating tolerance to LPS [65] and is protective in inflammation resulting from stroke [66]. Juang and colleagues reported that IRF3 nuclear translocation and activation can be prevented by 1 µg/ ml LPS from *E. coli* 055:B5 during simultaneous exposure to Newcastle disease virus, and this effect was reversed by overexpression of IRF3 [67].

4.4. LPS_{EC} and LPS_{SM} have diverse effects on U251 cellular proliferation and migration

TLR4 and its ligands are known to influence differentiation and proliferation of neural stem cells, and neuronal progenitor cells during development and in adulthood under physiological and pathological conditions [17, 68]. In contrast, the impact of TLR4 agonists on glioblastomas is controversial and a matter of an ongoing scientific debate. For example, while anti-tumoural effects of LPS has been reported *in vivo* [20], a tumour-promoting action (increase of proliferation and invasion) has been proposed *in vitro* for U118 and U87 cells [21]. Deciphering these observed differences is not helped by the fact that in the past, many studies have not reported the chemotype of LPS used in their studies. Interestingly, constitutively active NF-κB is known to play a pivotal role in glioblastoma cell proliferation and invasiveness [38, 69]. In contrast, apoptosis and reduced invasive behaviour, as well as decreased production of pro-angiogenic factors can be observed after overexpression of IRF3 [40]. Thus, our data could provide an explanation for the conflicting reports on the role of TLR4 signalling in glioma calls. NF-κB is known to promote glioma cell proliferation and migration [69], whereas IRF3 induces apoptosis [40]. In general accordance with the literature, our data showed that stimulation with LPS_{EC} led to an increase in cell number, whereas LPS_{SM} had no effect on cell number. These effects correlate with our results showing that LPS_{EC} induces higher NF-κB activity than LPS_{SM}. Previously, Westhoff and colleagues suggested that inhibition of NF-κB resulted in inhibition of glioma cell migration [39]. Therefore, we also examined migration of U251 cells following LPS treatment. Treatment with LPS_{SM} resulted in significant inhibition of migration, whereas stimulation with LPS_{EC} had no inhibitory effects. This LPS_{SM}-dependent inhibition is consistent

with our observation that LPS_{SM} leads to lower NF-κB activity than LPS_{EC}, whereas both chemotypes promote similar IRF3 activation.

4.5. LPS chemotypes do not affect TLR clustering or higher order oligomer formation

The spatial organisation of TLR4 at the cell membrane is involved in the activation of the respective downstream signalling [24, 41]. In order to investigate if the ligand dependent differences in the signalling are a result of changes in spatial organisation of the receptor at the plasma membrane, we applied *d*STORM super-resolution imaging. Due to the molecular-scale size of TLR4 and its clusters (< 200 nm) conventional microscopy cannot be applied to assess size and density of TLR4 on the membrane. In our study, we could not observe any significant differences in TLR4 abundance after treatment with different LPS chemotypes. However, we measured a remarkable cell-to-cell heterogeneity, ranging between 1.9 and 15.6 receptor clusters per µm². On average 7.0 ± 1.0 (SEM) TLR4 clusters per µm² were found in untreated cells (n=13), which is comparable to the density of other membrane receptors [70]. For other receptors, a formation of higher order oligomers after the respective ligand induction has been reported [30, 71]. For TLR4, Aaron and colleagues used *d*STORM to analyse potential ligand-dependent changes in TLR4 cluster size in haematopoietic cells. In their study, they reported a TLR4 cluster size of ~ 300 nm which increased to over 500 nm after LPS stimulation [72]. In contrast, we determined a TLR4 cluster size of ~ 50 nm in unstimulated cells. Moreover, we did not observe changes in cluster size following stimulation with either of the two LPS chemotypes (Fig. 4, Tables 1 and 2). One possible explanation for this discrepancy is the different cell lines used to quantify the TLR4 cluster size. While our study used U251 glioma cells line, P388D1 macrophage cell lines were used by Aaron et *al.*. An interesting note on extracting molecular-level clustering from SMLM data was recently reported by Burgert *et al.* [73], who investigated the influence of photoswitching rates on the appearance of clusters. They report that for high labelling densities in combination with inappropriate photoswitching rates, artificial clustering can occur in SMLM images. The reason behind this observation is that more than one fluorophore is active within a diffraction-limited region which leads to a false localization [74, 75]. In our study, we carefully adjusted the laser intensities to guarantee optimal photoswitching of Alexa Fluor 647. With these settings, we could not observe any difference in receptor density and cluster size prior or post LPS induction. We conclude that neither internalisation nor formation of higher order TLR4 oligomers play a decisive role in LPS-induced downstream signalling events.

4.6. Cholesterol-rich microdomains play a role in TLR4 signalling

In hematopoietic cells and cell lines TLR4 is known to be partly associated with cholesterol-rich membrane microdomains [25, 76] and can internalise via rafts/caveolae-mediated endocytosis in astrocytes [77]. In agreement with this, we show that TLR4 is partially co-

localised with CTx at the plasma membrane of U251 cells (Fig. 5A). Membrane microdomains have been suggested to play a role in TLR4 oligomerisation and downstream signalling [25]. Recently, Schoeninger and colleagues demonstrated that remodelling of macrophage cholesterol-rich microdomains using polyunsaturated fatty acids results in attenuated inflammatory signalling after TLR4 stimulation [76]. In our study, MCD treatment resulted in an early nuclear translocation of p65 and significantly increased sustained NF-κB activity in cells treated with LPS_{SM} compared to both LPS_{EC} treated and control cells (Fig. 5C-D). No increase in p65 translocation and sustained NF-κB activity was observed in cells exposed to LPS_{EC}. Notably, MCD-treatment has no effects on activity of IRF3 (Fig. 5C). These results suggest that microdomains play a decisive role in TLR4 mediated activation of MyD88- or TRIF-mediated signalling pathways. Interestingly, TLR4 can be internalised via rafts/caveolae in astrocytes [77]. Membrane microdomains were believed to have a size ranging from 10-200 nm [78] and cannot be resolved by confocal microscopy. Recently, we applied helium ion microscopy (HIM), atomic force microscopy and *d*STORM to visualize microdomains in the membranes of mammalians cells including neurons [79]. Both HIM and *d*STORM revealed a size of 10-50 nm. Notably, the TLR4 clusters detected in the present study are in similar range (~50 nm).

4.7. Implications for biased agonism of TLR4

Due to the broad range of TLR4-ligands including PAMPS but also DAMPs, precise regulation of the inflammatory balance could be an efficient way to control the cellular reaction. Indeed, investigation into the use of TLR agonists for therapeutic use is an area of great scientific interest (reviewed in [80]). According to this assumption, Morris and colleagues reported that the inflammatory balance is an intrinsic feature of TLR4 that allows monocytes to respond in a concentration-dependent manner to LPS [12]. Our study further proves that inflammatory balance of TLR4 signalling can be regulated not only in a concentration-dependent, but also in a ligand-dependent manner. The creation of a highly sensitive and specific signalling hub also raises the possibility that the potential of TLR4 as a therapeutic target might not be restricted to cellular responses following infection or tissue damage. TLR4 is expressed in many cancer types including head and neck, skin and breast cancer (reviewed in [81]) and is involved in tumour cell proliferation and migration, if the inflammatory balance is shifted towards NF-κB-dependent pro-inflammatory signalling. In this context, Nunez and colleagues reported that LPS induced and TLR4 mediated induction of IFNβ has a potent antitumoural activity in melanoma cells [82].

In conclusion, our results provide insights in the ligand-dependent intracellular responses mediated by TLR4. In particular, we show for the first time that natural TLR4 ligands can act as biased agonists, preferentially activating IRF3 over NF-κB in glioma cells. Notably, these

differences in downstream signalling are not dependent on the organization of the receptor on the membrane, as clustering cannot be seen under any condition with single-molecule localization microscopy. Here we show that high NF-κB activation in combination with moderate IRF3 activity promotes glioma cell proliferation. In contrast, low NF-κB and moderate IRF3 activity have no influence on glioma proliferation, but inhibit their migration potentially pointing towards future treatment of gliomas using TRIF-biased natural, synthetic or endogenous TLR4 ligands.

Acknowledgements

This study has been supported by grants of the DFG (German Research Foundation) to MH and DW (HE6166/9-1 and WI4318/2-1). We thank Barbara Kaltschmidt (Molecular Neurobiology, University of Bielefeld, Germany) and Christian Kaltschmidt (Cell Biology, University of Bielefeld, Germany) for support and critical discussion. We further thank Katherine A. Fitzgerald (Department of Medicine, University of Massachusetts Medical School, Worcester, USA) for kindly providing the IRF3 gene reporter system.

Author contributions

Conceived and designed the experiments: MH and DW. Performed the experiments: MZ, CK, KV and KB. Analysed the data: MZ, CK, KB, GC, MH and DW. Wrote the paper: MZ, CK, GC, MH and DW.

Conflict of interest

The authors declare that they have no competing interests.

References

[1] E.M. Moresco, D. LaVine, B. Beutler, Toll-like receptors, Curr Biol, 21 (2011) R488-493.
[2] J.C. Chow, D.W. Young, D.T. Golenbock, W.J. Christ, F. Gusovsky, Toll-like receptor-4 mediates lipopolysaccharide-induced signal transduction, J Biol Chem, 274 (1999) 10689-10692.
[3] B. Beutler, X. Du, A. Poltorak, Identification of Toll-like receptor 4 (Tlr4) as the sole conduit for LPS signal transduction: genetic and evolutionary studies, J Endotoxin Res, 7 (2001) 277-280.
[4] C.R. Casella, T.C. Mitchell, Inefficient TLR4/MD-2 heterotetramerization by monophosphoryl lipid A, PLoS One, 8 (2013) e62622.
[5] K.A. Fitzgerald, D.C. Rowe, B.J. Barnes, D.R. Caffrey, A. Visintin, E. Latz, B. Monks, P.M. Pitha, D.T. Golenbock, LPS-TLR4 signaling to IRF-3/7 and NF-kappaB involves the toll adapters TRAM and TRIF, J Exp Med, 198 (2003) 1043-1055.
[6] J.C. Kagan, T. Su, T. Horng, A. Chow, S. Akira, R. Medzhitov, TRAM couples endocytosis of Toll-like receptor 4 to the induction of interferon-beta, Nat Immunol, 9 (2008) 361-368.
[7] K.A. Fitzgerald, S.M. McWhirter, K.L. Faia, D.C. Rowe, E. Latz, D.T. Golenbock, A.J. Coyle, S.M. Liao, T. Maniatis, IKKepsilon and TBK1 are essential components of the IRF3 signaling pathway, Nat Immunol, 4 (2003) 491-496.

[8] A.I. Dragan, V.V. Hargreaves, E.N. Makeyeva, P.L. Privalov, Mechanisms of activation of interferon regulator factor 3: the role of C-terminal domain phosphorylation in IRF-3 dimerization and DNA binding, Nucleic Acids Res, 35 (2007) 3525-3534.
[9] Y.T. Juang, W. Lowther, M. Kellum, W.C. Au, R. Lin, J. Hiscott, P.M. Pitha, Primary activation of interferon A and interferon B gene transcription by interferon regulatory factor 3, Proc Natl Acad Sci U S A, 95 (1998) 9837-9842.
[10] L. Tarassishin, A. Bauman, H.S. Suh, S.C. Lee, Anti-viral and anti-inflammatory mechanisms of the innate immune transcription factor interferon regulatory factor 3: relevance to human CNS diseases, J Neuroimmune Pharmacol, 8 (2013) 132-144.
[11] M.C. Morris, E.A. Gilliam, L. Li, Innate immune programing by endotoxin and its pathological consequences, Front Immunol, 5 (2014) 680.
[12] M.C. Morris, E.A. Gilliam, J. Button, L. Li, Dynamic modulation of innate immune response by varying dosages of lipopolysaccharide (LPS) in human monocytic cells, J Biol Chem, 289 (2014) 21584-21590.
[13] S. Lehnardt, C. Lachance, S. Patrizi, S. Lefebvre, P.L. Follett, F.E. Jensen, P.A. Rosenberg, J.J. Volpe, T. Vartanian, The toll-like receptor TLR4 is necessary for lipopolysaccharide-induced oligodendrocyte injury in the CNS, J Neurosci, 22 (2002) 2478-2486.
[14] A. Rolls, R. Shechter, A. London, Y. Ziv, A. Ronen, R. Levy, M. Schwartz, Toll-like receptors modulate adult hippocampal neurogenesis, Nat Cell Biol, 9 (2007) 1081-1088.
[15] P. Wochal, V.A. Rathinam, A. Dunne, T. Carlson, W. Kuang, K.J. Seidl, J.P. Hall, L.L. Lin, M. Collins, S.A. Schattgen, C.R. MacKay, C.T. Fagundes, S. Carpenter, K.A. Fitzgerald, L.A. O'Neill, TRIL is involved in cytokine production in the brain following Escherichia coli infection, J Immunol, 193 (2014) 1911-1919.
[16] E. Okun, K.J. Griffioen, M.P. Mattson, Toll-like receptor signaling in neural plasticity and disease, Trends Neurosci, 34 (2011) 269-281.
[17] M. Zeuner, K. Bieback, D. Widera, Controversial Role of Toll-like Receptor 4 in Adult Stem Cells, Stem Cell Rev, 11 (2015) 621-634.
[18] D. Kaul, P. Habbel, K. Derkow, C. Kruger, E. Franzoni, F.G. Wulczyn, S. Bereswill, R. Nitsch, E. Schott, R. Veh, T. Naumann, S. Lehnardt, Expression of Toll-like receptors in the developing brain, PLoS One, 7 (2012) e37767.
[19] E. Okun, B. Barak, R. Saada-Madar, S.M. Rothman, K.J. Griffioen, N. Roberts, K. Castro, M.R. Mughal, M.A. Pita, A.M. Stranahan, T.V. Arumugam, M.P. Mattson, Evidence for a developmental role for TLR4 in learning and memory, PLoS One, 7 (2012) e47522.
[20] P. Gupta, S. Ghosh, A. Nagarajan, V.S. Mehta, E. Sen, beta-defensin-3 negatively regulates TLR4-HMGB1 axis mediated HLA-G expression in IL-1beta treated glioma cells, Cell Signal, 25 (2013) 682-689.
[21] V. Sarrazy, N. Vedrenne, F. Billet, N. Bordeau, S. Lepreux, A. Vital, M.O. Jauberteau, A. Desmouliere, TLR4 signal transduction pathways neutralize the effect of Fas signals on glioblastoma cell proliferation and migration, Cancer Lett, 311 (2011) 195-202.
[22] R. Tewari, S.R. Choudhury, S. Ghosh, V.S. Mehta, E. Sen, Involvement of TNFalpha-induced TLR4-NF-kappaB and TLR4-HIF-1alpha feed-forward loops in the regulation of inflammatory responses in glioma, J Mol Med (Berl), 90 (2012) 67-80.
[23] M.R. Chicoine, M. Zahner, E.K. Won, R.R. Kalra, T. Kitamura, A. Perry, R. Higashikubo, The in vivo antitumoral effects of lipopolysaccharide against glioblastoma multiforme are mediated in part by Toll-like receptor 4, Neurosurgery, 60 (2007) 372-380; discussion 381.
[24] S. Saitoh, S. Akashi, T. Yamada, N. Tanimura, F. Matsumoto, K. Fukase, S. Kusumoto, A. Kosugi, K. Miyake, Ligand-dependent Toll-like receptor 4 (TLR4)-oligomerization is directly linked with TLR4-signaling, J Endotoxin Res, 10 (2004) 257-260.
[25] S.W. Wong, M.J. Kwon, A.M. Choi, H.P. Kim, K. Nakahira, D.H. Hwang, Fatty acids modulate Toll-like receptor 4 activation through regulation of receptor dimerization and recruitment into lipid rafts in a reactive oxygen species-dependent manner, J Biol Chem, 284 (2009) 27384-27392.
[26] F. Bachelerie, J. Alcami, F. Arenzana-Seisdedos, J.L. Virelizier, HIV enhancer activity perpetuated by NF-kappa B induction on infection of monocytes, Nature, 350 (1991) 709-712.

[27] J. Schindelin, I. Arganda-Carreras, E. Frise, V. Kaynig, M. Longair, T. Pietzsch, S. Preibisch, C. Rueden, S. Saalfeld, B. Schmid, J.Y. Tinevez, D.J. White, V. Hartenstein, K. Eliceiri, P. Tomancak, A. Cardona, Fiji: an open-source platform for biological-image analysis, Nat Methods, 9 (2012) 676-682.
[28] A.P. Piehler, R.M. Grimholt, R. Ovstebo, J.P. Berg, Gene expression results in lipopolysaccharide-stimulated monocytes depend significantly on the choice of reference genes, BMC Immunol, 11 (2010) 21.
[29] C.C. Liang, A.Y. Park, J.L. Guan, In vitro scratch assay: a convenient and inexpensive method for analysis of cell migration in vitro, Nat Protoc, 2 (2007) 329-333.
[30] F. Fricke, S. Malkusch, G. Wangorsch, J.F. Greiner, B. Kaltschmidt, C. Kaltschmidt, D. Widera, T. Dandekar, M. Heilemann, Quantitative single-molecule localization microscopy combined with rule-based modeling reveals ligand-induced TNF-R1 reorganization toward higher-order oligomers, Histochem Cell Biol, 142 (2014) 91-101.
[31] S. Wolter, A. Loschberger, T. Holm, S. Aufmkolk, M.C. Dabauvalle, S. van de Linde, M. Sauer, rapidSTORM: accurate, fast open-source software for localization microscopy, Nat Methods, 9 (2012) 1040-1041.
[32] S. Malkusch, W. Muranyi, B. Muller, H.G. Krausslich, M. Heilemann, Single-molecule coordinate-based analysis of the morphology of HIV-1 assembly sites with near-molecular spatial resolution, Histochem Cell Biol, 139 (2013) 173-179.
[33] S. Deng, S. Zhu, Y. Qiao, Y.J. Liu, W. Chen, G. Zhao, J. Chen, Recent advances in the role of toll-like receptors and TLR agonists in immunotherapy for human glioma, Protein Cell, 5 (2014) 899-911.
[34] A. Furstenberg, M. Heilemann, Single-molecule localization microscopy-near-molecular spatial resolution in light microscopy with photoswitchable fluorophores, Phys Chem Chem Phys, 15 (2013) 14919-14930.
[35] M. Heilemann, S. van de Linde, M. Schuttpelz, R. Kasper, B. Seefeldt, A. Mukherjee, P. Tinnefeld, M. Sauer, Subdiffraction-resolution fluorescence imaging with conventional fluorescent probes, Angew Chem Int Ed Engl, 47 (2008) 6172-6176.
[36] U. Endesfelder, S. Malkusch, F. Fricke, M. Heilemann, A simple method to estimate the average localization precision of a single-molecule localization microscopy experiment, Histochem Cell Biol, 141 (2014) 629-638.
[37] A. Hoffmann, A. Levchenko, M.L. Scott, D. Baltimore, The IkappaB-NF-kappaB signaling module: temporal control and selective gene activation, Science, 298 (2002) 1241-1245.
[38] D. Smith, T. Shimamura, S. Barbera, B.E. Bejcek, NF-kappaB controls growth of glioblastomas/astrocytomas, Mol Cell Biochem, 307 (2008) 141-147.
[39] M.A. Westhoff, S. Zhou, L. Nonnenmacher, G. Karpel-Massler, C. Jennewein, M. Schneider, M.E. Halatsch, N.O. Carragher, B. Baumann, A. Krause, T. Simmet, M.G. Bachem, C.R. Wirtz, K.M. Debatin, Inhibition of NF-kappaB signaling ablates the invasive phenotype of glioblastoma, Mol Cancer Res, 11 (2013) 1611-1623.
[40] L. Tarassishin, S.C. Lee, Interferon regulatory factor 3 alters glioma inflammatory and invasive properties, J Neurooncol, 113 (2013) 185-194.
[41] A. Plociennikowska, A. Hromada-Judycka, K. Borzecka, K. Kwiatkowska, Co-operation of TLR4 and raft proteins in LPS-induced pro-inflammatory signaling, Cell Mol Life Sci, 72 (2015) 557-581.
[42] B.D. Ripley, Modelling spatial patterns, Journal of the Royal Statistical Society. Series B (Methodological), (1977) 172-212.
[43] T. Kawai, O. Adachi, T. Ogawa, K. Takeda, S. Akira, Unresponsiveness of MyD88-deficient mice to endotoxin, Immunity, 11 (1999) 115-122.
[44] D. Widera, A. Kaus, C. Kaltschmidt, B. Kaltschmidt, Neural stem cells, inflammation and NF-kappaB: basic principle of maintenance and repair or origin of brain tumours?, J Cell Mol Med, 12 (2008) 459-470.
[45] L. Tarassishin, H.S. Suh, S.C. Lee, Interferon regulatory factor 3 plays an anti-inflammatory role in microglia by activating the PI3K/Akt pathway, J Neuroinflammation, 8 (2011) 187.

[46] E.S. Gudo, S.D. Silva-Barbosa, L. Linhares-Lacerda, M. Ribeiro-Alves, S.C. Real, D.C. Bou-Habib, W. Savino, HAM/TSP-derived HTLV-1-infected T cell lines promote morphological and functional changes in human astrocytes cell lines: possible role in the enhanced T cells recruitment into Central Nervous System, Virol J, 12 (2015) 165.
[47] Z. Jiang, P. Georgel, X. Du, L. Shamel, S. Sovath, S. Mudd, M. Huber, C. Kalis, S. Keck, C. Galanos, M. Freudenberg, B. Beutler, CD14 is required for MyD88-independent LPS signaling, Nat Immunol, 6 (2005) 565-570.
[48] Z. Yang, M.A. Breider, R.C. Carroll, M.S. Miller, P.N. Bochsler, Soluble CD14 and lipopolysaccharide-binding protein from bovine serum enable bacterial lipopolysaccharide-mediated cytotoxicity and activation of bovine vascular endothelial cells in vitro, J Leukoc Biol, 59 (1996) 241-247.
[49] L.M. Luttrell, S. Maudsley, L.M. Bohn, Fulfilling the Promise of "Biased" G Protein-Coupled Receptor Agonism, Mol Pharmacol, 88 (2015) 579-588.
[50] A.S. Pupo, D.A. Duarte, V. Lima, L.B. Teixeira, E.S.L.T. Parreiras, C.M. Costa-Neto, Recent updates on GPCR biased agonism, Pharmacol Res, (2016).
[51] K.J. Wilson, J.L. Gilmore, J. Foley, M.A. Lemmon, D.J. Riese, 2nd, Functional selectivity of EGF family peptide growth factors: implications for cancer, Pharmacol Ther, 122 (2009) 1-8.
[52] T.B. Salisbury, J.K. Tomblin, Insulin/Insulin-like growth factors in cancer: new roles for the aryl hydrocarbon receptor, tumor resistance mechanisms, and new blocking strategies, Front Endocrinol (Lausanne), 6 (2015) 12.
[53] C.R. Keenan, M.J. Lew, A.G. Stewart, Biased signalling from the glucocorticoid receptor: Renewed opportunity for tailoring glucocorticoid activity, Biochem Pharmacol, (2016).
[54] F. De Smet, A. Christopoulos, P. Carmeliet, Allosteric targeting of receptor tyrosine kinases, Nat Biotechnol, 32 (2014) 1113-1120.
[55] P.R. Gentry, P.M. Sexton, A. Christopoulos, Novel Allosteric Modulators of G Protein-coupled Receptors, J Biol Chem, 290 (2015) 19478-19488.
[56] V. Mata-Haro, C. Cekic, M. Martin, P.M. Chilton, C.R. Casella, T.C. Mitchell, The vaccine adjuvant monophosphoryl lipid A as a TRIF-biased agonist of TLR4, Science, 316 (2007) 1628-1632.
[57] C. Cekic, C.R. Casella, C.A. Eaves, A. Matsuzawa, H. Ichijo, T.C. Mitchell, Selective activation of the p38 MAPK pathway by synthetic monophosphoryl lipid A, J Biol Chem, 284 (2009) 31982-31991.
[58] W.S. Bowen, L.A. Minns, D.A. Johnson, T.C. Mitchell, M.M. Hutton, J.T. Evans, Selective TRIF-dependent signaling by a synthetic toll-like receptor 4 agonist, Sci Signal, 5 (2012) ra13.
[59] J.P. Kolb, C.R. Casella, S. SenGupta, P.M. Chilton, T.C. Mitchell, Type I interferon signaling contributes to the bias that Toll-like receptor 4 exhibits for signaling mediated by the adaptor protein TRIF, Sci Signal, 7 (2014) ra108.
[60] X.A. Wang, R. Zhang, Z.G. She, X.F. Zhang, D.S. Jiang, T. Wang, L. Gao, W. Deng, S.M. Zhang, L.H. Zhu, S. Guo, K. Chen, X.D. Zhang, D.P. Liu, H. Li, Interferon regulatory factor 3 constrains IKKbeta/NF-kappaB signaling to alleviate hepatic steatosis and insulin resistance, Hepatology, 59 (2014) 870-885.
[61] S.M. Zughaier, S.M. Zimmer, A. Datta, R.W. Carlson, D.S. Stephens, Differential induction of the toll-like receptor 4-MyD88-dependent and -independent signaling pathways by endotoxins, Infect Immun, 73 (2005) 2940-2950.
[62] A.C. Salyer, G. Caruso, K.K. Khetani, L.M. Fox, S.S. Malladi, S.A. David, Identification of Adjuvantic Activity of Amphotericin B in a Novel, Multiplexed, Poly-TLR/NLR High-Throughput Screen, PLoS One, 11 (2016) e0149848.
[63] M. Iwanaszko, M. Kimmel, NF-kappaB and IRF pathways: cross-regulation on target genes promoter level, BMC Genomics, 16 (2015) 307.
[64] G. Mathiak, K. Kabir, G. Grass, H. Keller, E. Steinringer, T. Minor, C. Rangger, L.F. Neville, Lipopolysaccharides from different bacterial sources elicit disparate cytokine responses in whole blood assays, Int J Mol Med, 11 (2003) 41-44.

[65] S.K. Biswas, P. Bist, M.K. Dhillon, T. Kajiji, C. Del Fresno, M. Yamamoto, E. Lopez-Collazo, S. Akira, V. Tergaonkar, Role for MyD88-independent, TRIF pathway in lipid A/TLR4-induced endotoxin tolerance, J Immunol, 179 (2007) 4083-4092.
[66] K.B. Vartanian, S.L. Stevens, B.J. Marsh, R. Williams-Karnesky, N.S. Lessov, M.P. Stenzel-Poore, LPS preconditioning redirects TLR signaling following stroke: TRIF-IRF3 plays a seminal role in mediating tolerance to ischemic injury, J Neuroinflammation, 8 (2011) 140.
[67] Y.T. Juang, W.C. Au, W. Lowther, J. Hiscott, P.M. Pitha, Lipopolysaccharide inhibits virus-mediated induction of interferon genes by disruption of nuclear transport of interferon regulatory factors 3 and 7, J Biol Chem, 274 (1999) 18060-18066.
[68] A. Moraga, J.M. Pradillo, M.I. Cuartero, M. Hernandez-Jimenez, M. Oses, M.A. Moro, I. Lizasoain, Toll-like receptor 4 modulates cell migration and cortical neurogenesis after focal cerebral ischemia, FASEB J, 28 (2014) 4710-4718.
[69] B. Raychaudhuri, Y. Han, T. Lu, M.A. Vogelbaum, Aberrant constitutive activation of nuclear factor kappaB in glioblastoma multiforme drives invasive phenotype, J Neurooncol, 85 (2007) 39-47.
[70] M.S. Dietz, F. Fricke, C.L. Kruger, H.H. Niemann, M. Heilemann, Receptor-ligand interactions: binding affinities studied by single-molecule and super-resolution microscopy on intact cells, Chemphyschem, 15 (2014) 671-676.
[71] L. Tarancon Diez, C. Bonsch, S. Malkusch, Z. Truan, M. Munteanu, M. Heilemann, O. Hartley, U. Endesfelder, A. Furstenberg, Coordinate-based co-localization-mediated analysis of arrestin clustering upon stimulation of the C-C chemokine receptor 5 with RANTES/CCL5 analogues, Histochem Cell Biol, 142 (2014) 69-77.
[72] J.S. Aaron, B.D. Carson, J.A. Timlin, Characterization of differential Toll-like receptor responses below the optical diffraction limit, Small, 8 (2012) 3041-3049.
[73] A. Burgert, S. Letschert, S. Doose, M. Sauer, Artifacts in single-molecule localization microscopy, Histochem Cell Biol, 144 (2015) 123-131.
[74] S. van de Linde, S. Wolter, M. Heilemann, M. Sauer, The effect of photoswitching kinetics and labeling densities on super-resolution fluorescence imaging, J Biotechnol, 149 (2010) 260-266.
[75] U. Endesfelder, M. Heilemann, Art and artifacts in single-molecule localization microscopy: beyond attractive images, Nat Methods, 11 (2014) 235-238.
[76] A. Schoeniger, H. Fuhrmann, J. Schumann, LPS- or Pseudomonas aeruginosa-mediated activation of the macrophage TLR4 signaling cascade depends on membrane lipid composition, PeerJ, 4 (2016) e1663.
[77] M. Pascual-Lucas, S. Fernandez-Lizarbe, J. Montesinos, C. Guerri, LPS or ethanol triggers clathrin- and rafts/caveolae-dependent endocytosis of TLR4 in cortical astrocytes, J Neurochem, 129 (2014) 448-462.
[78] L.J. Pike, The challenge of lipid rafts, J Lipid Res, 50 Suppl (2009) S323-328.
[79] M. Schurmann, N. Frese, A. Beyer, P. Heimann, D. Widera, V. Monkemoller, T. Huser, B. Kaltschmidt, C. Kaltschmidt, A. Golzhauser, Helium Ion Microscopy Visualizes Lipid Nanodomains in Mammalian Cells, Small, 11 (2015) 5781-5789.
[80] S. Gnjatic, N.B. Sawhney, N. Bhardwaj, Toll-like receptor agonists: are they good adjuvants?, Cancer J, 16 (2010) 382-391.
[81] C.W. Mai, Y.B. Kang, M.R. Pichika, Should a Toll-like receptor 4 (TLR-4) agonist or antagonist be designed to treat cancer? TLR-4: its expression and effects in the ten most common cancers, Onco Targets Ther, 6 (2013) 1573-1587.
[82] N.G. Nunez, V. Andreani, M.I. Crespo, D.A. Nocera, M.L. Breser, G. Moron, L. Dejager, C. Libert, V. Rivero, M. Maccioni, IFNbeta produced by TLR4-activated tumor cells is involved in improving the antitumoral immune response, Cancer Res, 72 (2012) 592-603.

Figure legends

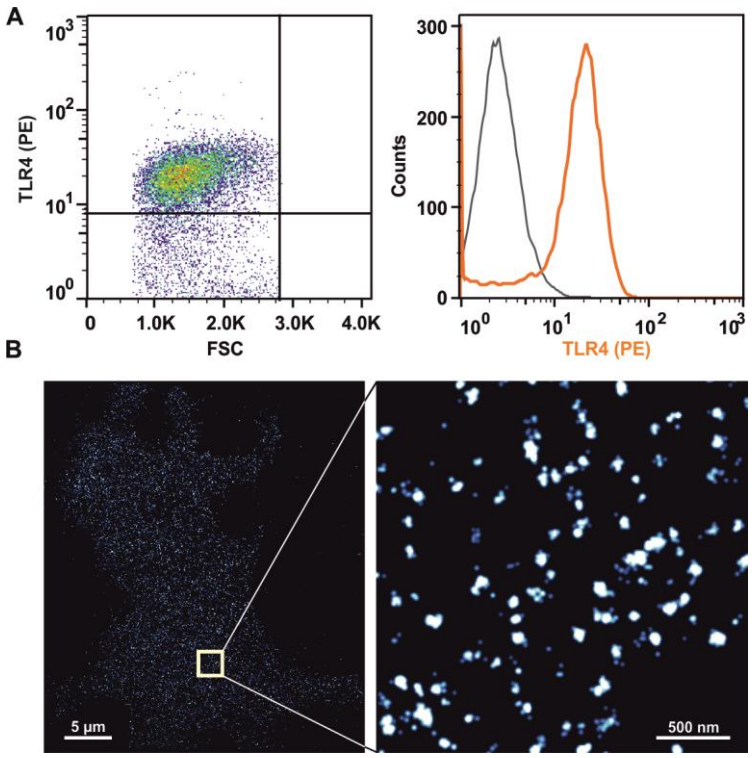

Figure 1. Clusters of TLR4 are uniformly distributed in the membrane of U251 cells. **A.** To verify the expression of TLR4 in U251 glioma cell, cells were incubated with an anti-TLR4 antibody without permeabilisation step and processed for flow cytometry revealing high expression of TLR4 at the membrane. Left: dot plot, FSC: forward scatter. Right: histogram. Orange: anti-TLR4, black: control. **B.** Direct stochastic optical reconstruction microscopy (*d*STORM) was applied to investigate the nano-spatial organization of TLR4 at the membrane of U251 cells stained with an anti TLR4 primary antibody and AlexaFluor647 as detection antibody. We found that TLR4 is uniformly distributed across the membrane and exhibits a density of 7.0 ± 1.0 receptor clusters / µm^2.

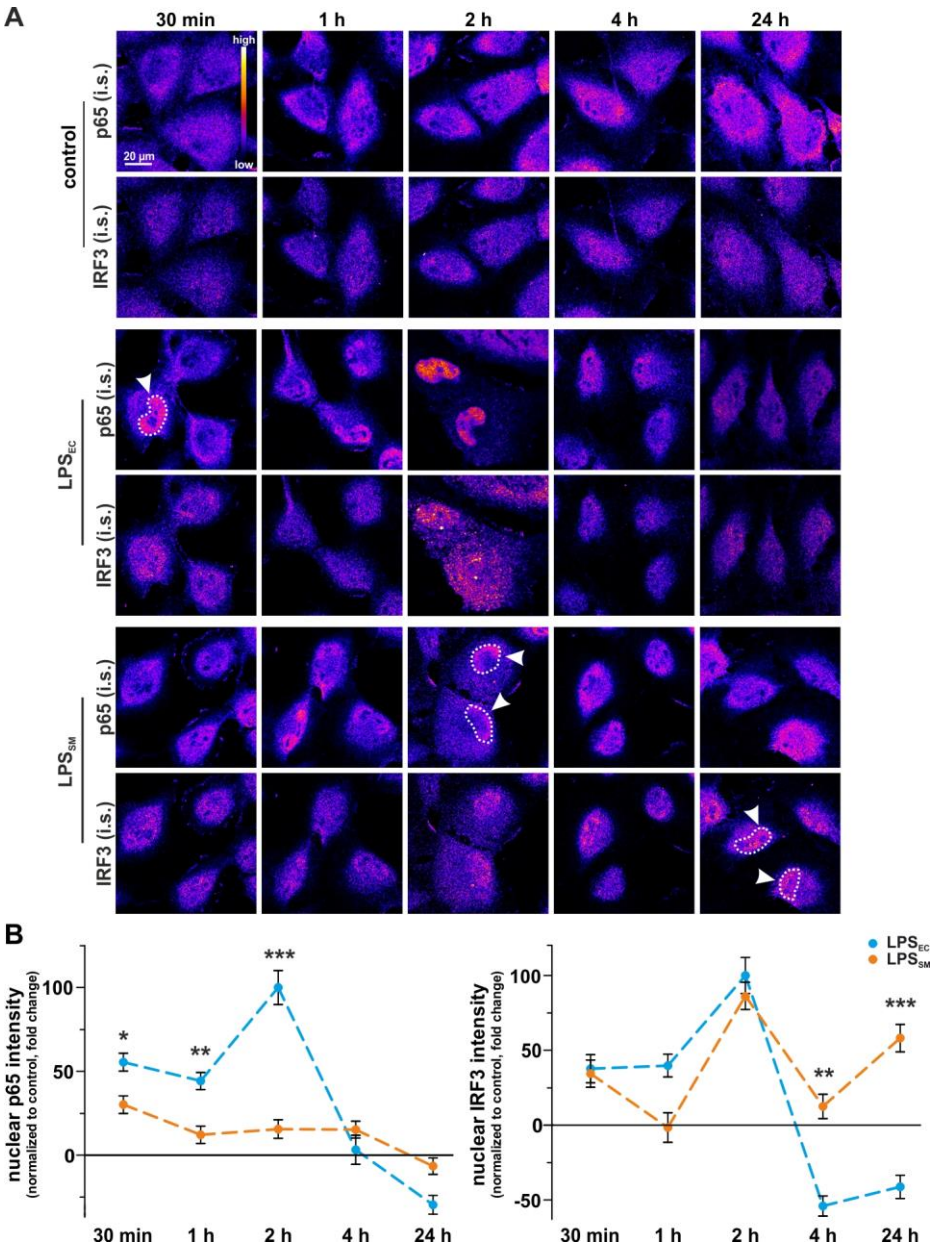

Figure 2. Kinetics of TLR4-induced nuclear translocation of IRF3 and NF-κB are ligand-dependent. **A.** In order to determine if the chemotype of the LPS affects the kinetics of nuclear translocation of NF-κB and IRF3, control cells and cells exposed to LPS_{SM} or LPS_{EC} were fixed at the indicated time points and co-stained for IRF3 and NF-κB subunit p65. **B.** Quantification of nuclear p65 and IRF3. We found that LPS_{EC} promotes rapid nuclear translocation of p65 (30 min, arrowhead). In cells stimulated with LPS_{SM} only low levels of nuclear NF-κB were observed at 2 h (arrowheads). Note the lower levels of nuclear p65 in cells treated with LPS_{SM} at all time points and reached the maximum after 24 h (arrows). In contrast, the levels of nuclear IRF3 were significantly higher in LPS_{SM}-treated cells in comparison to LPS_{EC} at both 4 and 24 h. The values represent means ± SEM. All experiments were performed in triplicate. **P*<0.05, ** *P*<0.01, ****P*<0.001.

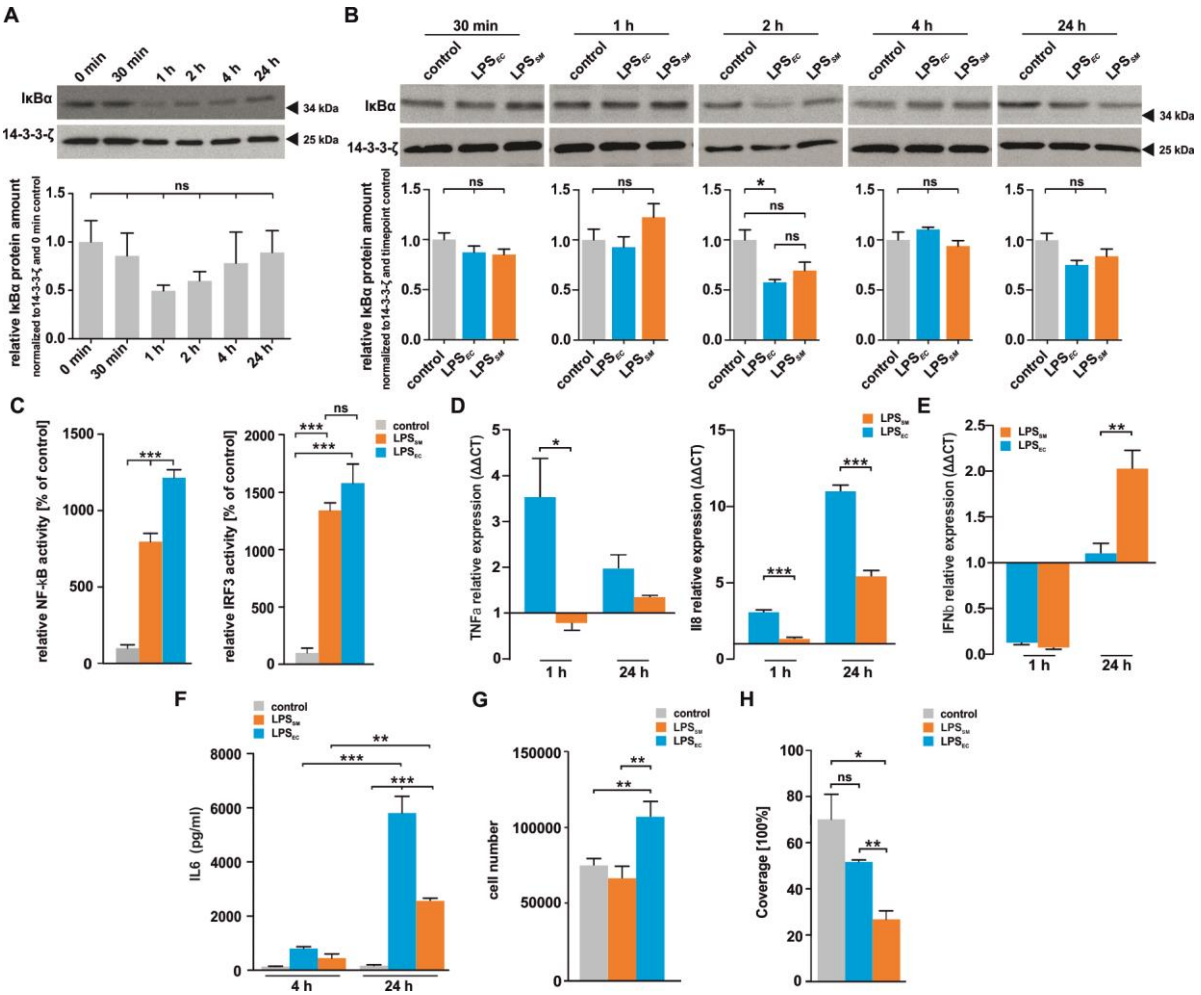

Figure 3. LPS_{EC} leads to MyD88-biased signalling and triggers U251 glioma cell proliferation, whereas LPS_{SM} stimulation results in a weak activation of NF-κB and inhibits migration. **A-B.** Cells were serum-starved to set a low baseline of active NF-κB (time point 0, panel A). Medium was changed to fresh serum-containing media with and without LPS for the indicated time. Samples were subjected to Western blotting to determine the basal-serum induced degradation of IκBα (A) and after LPS treatment (B). Representative Western blots are shown. Densitometric analysis was performed to semi-quantitatively determine the relative abundances of IκBα relative to that of 14-3-3-ζ. Normalisation was performed to respective relative abundances of IκBα in untreated cells at each time point. Significantly stronger IκBα degradation was detected after 2h treatment with LPS_{EC} compared to untreated control. Data are mean values of three independent experiments ± SEM. **P*<0.05. **C.** Cells were transiently transfected with NF-κB and IRF3 driven luciferase reporter plasmids followed by stimulation with LPS and detection of luciferase activity. Note the significantly higher NF-κB activity in LPS_{EC} treated cells compared to control and cell exposed to LPS_{SM} and no significantly different IRF3 activity after exposure to both LPS chemotypes. All experiments were performed in triplicate, data is displayed as mean ± SEM. ****P*<0.001. **D-E.** RT-qPCR was performed using mRNA isolated from cells treated with LPS 1h or 24h. Normalisation was

performed for all samples using GAPDH expression and untreated control approach (ΔΔCT). Data is displayed as mean of three independent experiments ± SEM. *P<0.05, ** P<0.01, ***P<0.001. Note that the pro-inflammatory NF-κB target genes TNF-α and IL8 are expressed at significantly higher level after treatment with $LPS_{EC,}$ whereas LPS_{SM} results in higher transcription of the IRF3 target gene IFNβ. **F.** ELISA was applied to measure LPS-induced secretion of the pro-inflammatory IL6 into the medium. We found that treatment with LPS_{EC} leads to significantly increased secretion of IL6 compared to control and cells exposed to $LPS_{SM.}$ Data represents three independent experiments ± SEM. ** P<0.01. **G.** Total cell number was determined after 3 days of culture in presence of LPS_{SM} or $LPS_{EC.}$ Treatment with LPS_{EC} leads to significantly higher proliferation, whereas we found no significant change of proliferation in cells after stimulation with LPS_{SM}. The values represent means of three independent experiments ± SEM. ** P<0.01. **H.** Wound healing assay was performed to determine the influence of LPS chemotype on U251 cell migration. In contrast to LPS_{EC}, LPS_{SM} significantly inhibits U251 migration. Data are mean values of three independent experiments ± SEM. ** P<0.01, ***P<0.001

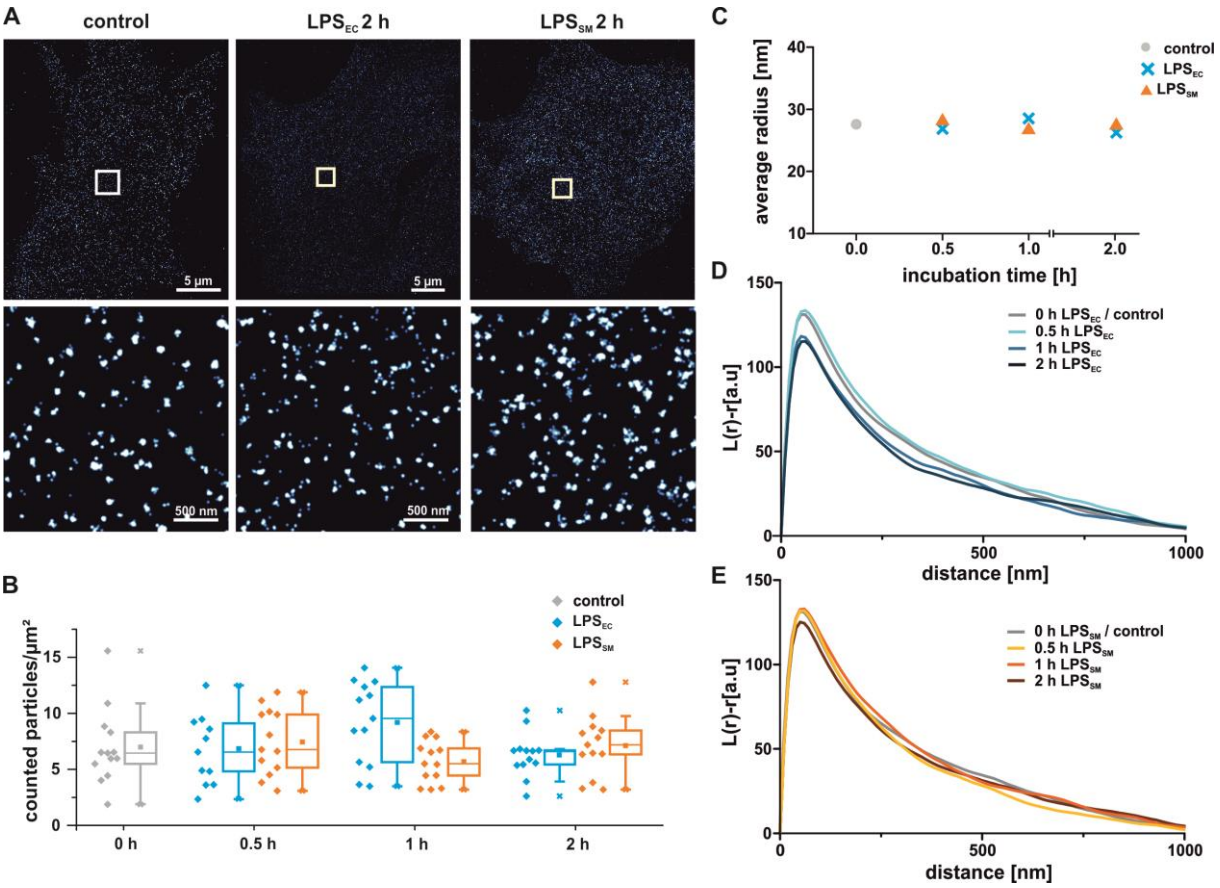

Figure 4. Distribution and size of TLR4 receptor clusters in U251 cells before and after induction with LPS. **A.** Representative *d*STORM images of immunostained TLR4 receptor clusters on the membrane of U251 cells. Super-resolution images are shown for a cell after treatment with LPS_{EC} for 2 h and LPS_{SM} for 2 h, respectively. A magnified view of the boxed regions is given for each cell. For both LPS_{EC} and LPS_{SM}, the receptor is uniformly distributed across the plasma membrane. **B.** Box plot of the number of TLR4 receptor clusters per µm² before and after incubation with LPS_{EC} or LPS_{SM}. For each condition the result of every single cells is shown (n=13). **C.** Ripley clustering analysis of the single molecule localization data sets of TLR4 receptors on U251 cells after applying LPS_{EC}. The maxima of the Ripley function indicate the cluster size. **D.** Ripley clustering analysis of TLR4 receptors in cells treated with LPS_{SM}. **D.** TLR4 receptor cluster sizes on the plasma membrane of U251 cells calculated with imaged-based cluster analysis. For each incubation time the radius of each receptor cluster was determined and averaged.

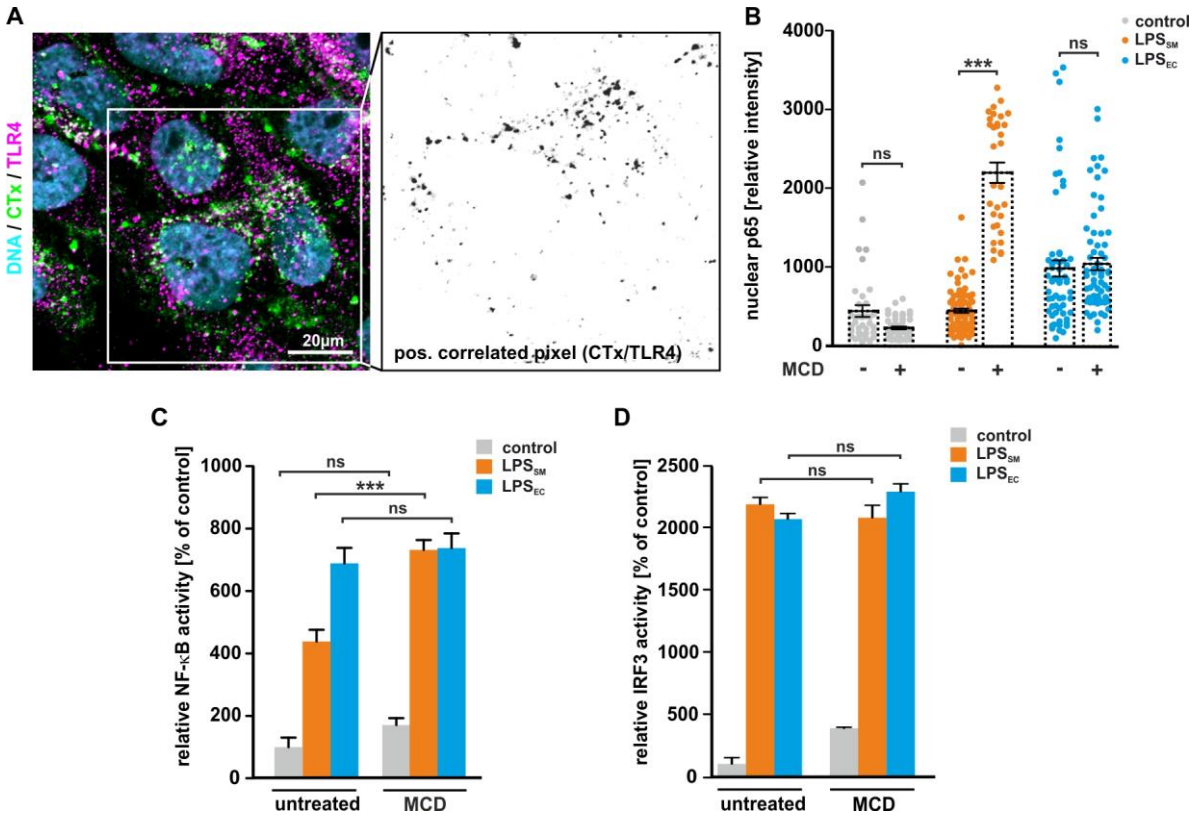

Figure 5. MCD induced depletion of cholesterol-rich membrane microdomains increases LPS$_{SM}$ induced NF-κB activity, but neither influences LPS$_{EC}$-mediated NF-κB activation nor IRF3 activity driven by both LPS chemotypes. **A**. To investigate potential co-localisation of TLR4 with cholesterol-rich membrane microdomains, cells were co-labelled with an anti TLR4 antibody and AlexaFluor488 conjugated Cholera Toxin subunit B (CTx). Analysis revealed a partial co-localisation of TLR4 and CTx. **B.** U251 cells were treated with MCD followed by a wash-out and exposure to both LPS chemotypes for 30 min followed by immunocytochemical staining for NF-κB subunit p65 and analysis of nuclear signal. Quantitative analysis of nuclear p65 shows significantly increased amount of nuclear p65 in cells treated with MCD and LPS$_{SM}$ but no significant differences in LPS$_{EC}$ induced nuclear translocation of p65. The values represent means ± SEM. All experiments were performed in triplicate. ***P<0.001. **C.** U251 cells transiently transfected with NF-κB and IRF3 reported plasmids were treated with MCD and LPS and processed for analysis of bioluminescence. Note that treatment with MCD / LPS$_{SM}$ significantly increased NF-κB driven luciferase activity compared to LPS$_{SM\ alone}$ and control, but has no effect on IRF3 driven bioluminescence. Data displayed as mean of three independent experiments ± SEM. ***P<0.001.

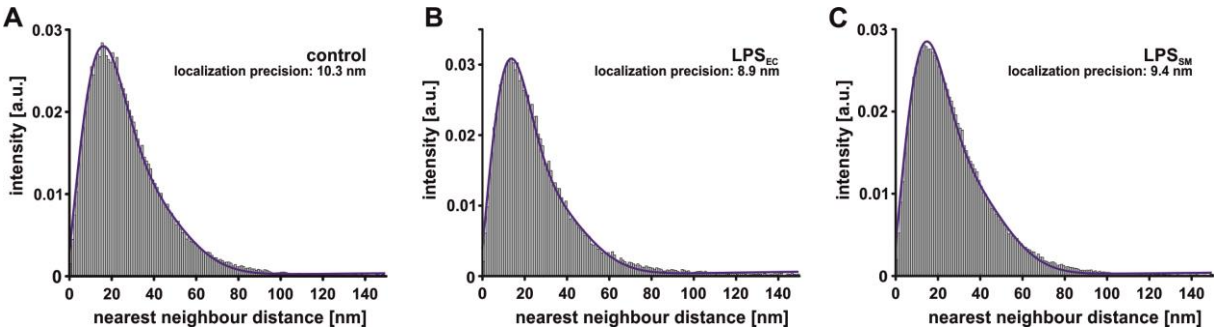

Figure S1. Localization precision of the dSTORM images. Localization precision was determined using nearest neighbour analysis [36] for a single cell. **A.** Control. **B.** Induction with LPS_{EC}. **C.** Induction with LPS_{SM} .The localization precision ranges from 8.9 nm to 10.3 nm.

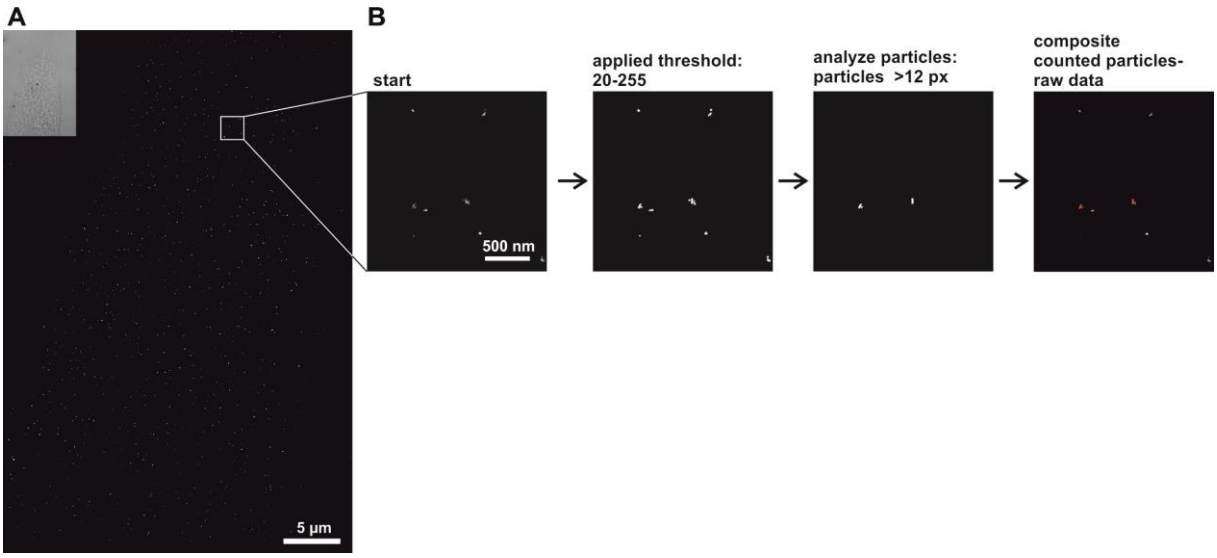

Figure S2. Principle of image-based cluster analysis. **A.** SMLM image of a U251 cell which was labelled with the secondary antibody only (negative control; inset shows bright-field image). On average, 0.3 ± 0.1 particles per µm² were found. **B**. An intensity threshold is applied to the raw image (boxed region from **A**) and particles composed of at least 12 pixels are counted. The composite image (right) shows an overlay of the raw image (white) and the identified particles (red).

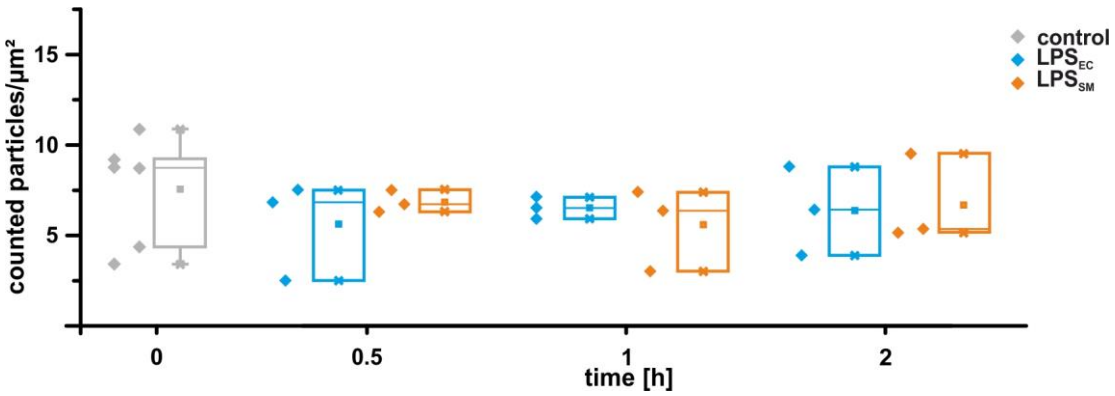

Figure S3. Results of single-molecule localization microscopy are consistent for different primary antibodies. A. Control experiment with different primary antibody (ab32518, Abcam, UK). Box plot shows the number of TLR4 receptor clusters per µm² for each time point before and after incubation with LPS_{EC} or LPS_{SM}.

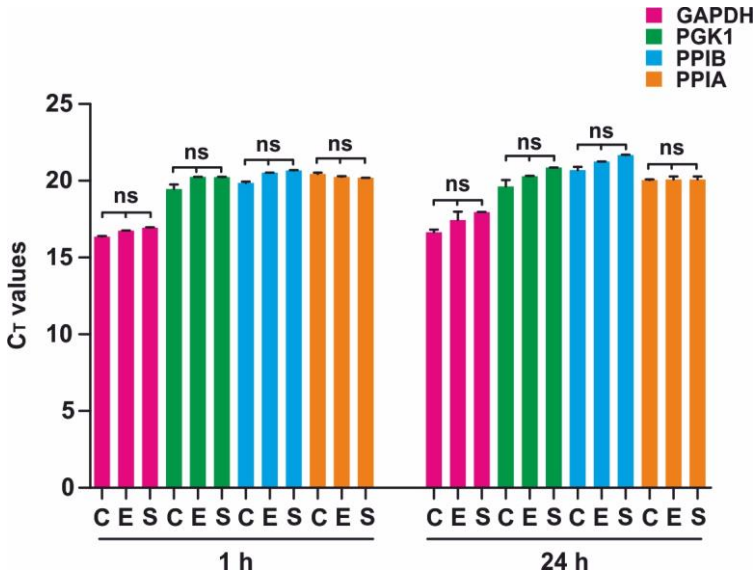

Figure S4. GAPDH expression is not regulated by TLR4 in U251 glioma cells. RT-qPCR was performed using mRNA isolated from cells treated with both LPS chemotypes for 1h or 24h. Statistical analysis was performed to assess the potential regulation of the reference genes by TLR4-mediated signalling cascades. Note that neither GAPDH nor the control reference genes PGK1, PPIB, and PPIA were regulated by the LPS treatment. C: control, E: LPS_{EC}, S: $LPS_{SM.}$

Table 1. Average number of TLR4 receptors per µm² on the plasma membrane of U251 cells before and after applying LPS. The cluster numbers were determined using image-based analysis of *d*STORM images. Numbers are average values determined from 13 cells per condition (SEM is given for each value).

Condition	**Number of TLR4 clusters per µm²**
TLR4 only	7.0 ± 1.0
TLR4 + LPS_{EC} 0.5 h	6.8 ± 0.8
TLR4 + LPS_{EC} 1 h	9.2 ± 1.0
TLR4 + LPS_{EC} 2 h	6.3 ± 0.5
TLR4 + LPS_{SM} 0.5 h	7.4 ± 0.8
TLR4 + LPS_{SM} 1 h	5.7 ± 0.5
TLR4 + LPS_{SM} 2 h	7.1 ± 0.8

Table 2. TLR4 receptor cluster sizes on cell membrane of U251 cells. Cluster size was calculated using imaged based analysis (radius) and coordinate based analysis (Ripley's H-function) before and after applying LPS_{EC} and LPS_{SM} for the indicated time points (SEM is given for each value).

Condition	Cluster radius [nm]	Maximum Ripley's H-function [nm]
TLR4 only	27.6 ± 0.04	54.7 ± 1.3
TLR4 + LPS_{EC} 0.5 h	26.9 ± 0.04	57.2 ± 1.7
TLR4 + LPS_{EC} 1 h	28.5 ± 0.04	56.3 ± 1.2
TLR4 + LPS_{EC} 2 h	26.2 ± 0.03	52.3 ± 1.2
TLR4 + LPS_{SM} 0.5 h	28.1 ± 0.03	57.4 ± 1.7
TLR4 + LPS_{SM} 1 h	26.7 ± 0.04	52.6 ± 0.9
TLR4 + LPS_{SM} 2 h	27.4 ± 0.04	55.7 ± 1.0

Table S1. Control experiment with different primary antibody. Numbers of average TLR4 receptors per µm² for each condition (n=6 for control condition, all other conditions: n=3).

Condition	Number of TLR4 clusters per µm²
TLR4 only	7.6 ± 1.2
TLR4 + LPS_{EC} 0.5 h	5.6 ± 1.6
TLR4 + LPS_{EC} 1 h	6.5 ± 0.4
TLR4 + LPS_{EC} 2 h	6.4 ± 1.4
TLR4 + LPS_{SM} 0.5 h	7.0 ± 0.4
TLR4 + LPS_{SM} 1 h	5.6 ± 1.3
TLR4 + LPS_{SM} 2 h	6.7 ± 1.4